MAPAN-Journal of Metrology Society of India (December 2022) 37(4):793–809
https://doi.org/10.1007/s12647-022-00583-0

ORIGINAL ARTICLE

Optical Noninvasive Temperature Measurement of Molten Melts in Metallurgical Process: A Review

X. Wu[1,2], J. Li[3], F. Liu[1]*, C. Liao[4], S. Chen[4]* and X. Wang[5]

[1]School of Electrical Engineering and Automation, Jiangxi University of Science and Technology, Ganzhou 341000, China

[2]Jiangxi Ionic Rare Earth Engineering Research Co. Led., Ganzhou 341000, China

[3]School of Mechanical and Electrical Engineering, Jiangxi University of Science and Technology, Ganzhou 341000, China

[4]Faculty of Materials Metallurgy and Chemistry, Jiangxi University of Science and Technology, Ganzhou 341000, China

[5]School of Resources and Environmental Engineering, Jiangxi University of Science and Technology, Ganzhou 341000, China

Received: 04 March 2022 / Accepted: 29 June 2022 / Published online: 25 July 2022

Abstract: High-temperature melts, including molten metals and molten melts, are common substances in the pyrometallurgical process. Temperature is one of the most concerned and important physical properties of melts. Maintaining a melt's molten state means huge energy consumption. Moreover, the temporary storage, transfer, and subsequent processing of them are usually accompanied by considerable risks. Thus, real-time temperature measurement of the melt is one of the core requirements. Due to the high corrosiveness of molten phases, invasive temperature measurement is no longer applicable or even could not deploy in high-temperature melts. Therefore, optical temperature measurement technology has been brought into prime focus. This paper provides a review of the academic improvement involved and commercial technology employed in each optical temperature measurement device. Recent progress and trends are investigated in both radiation thermometers and computer vision-based pyrometers. The measurement principle and characteristics of each device are discussed in detail. The optimization of accuracy is emphasized based on radiation thermometers, while the reasons for a few computer vision-based pyrometers are mentioned. In addition, a new temperature diagnosis technology that combines computer vision and artificial intelligence has received widespread attention and applications in recent years. Future developments are briefly introduced to provide some insight into which direction the development and application of temperature measurement technologies are likely to develop.

Keywords: Optical temperature measurement; High-temperature melts; CCD image; Radiation thermometer

1. Introduction

Temperature is the most significant thermodynamic state quantity determined in industrial processes, and it plays an important role in various aspects such as process stability, high quality, and energy saving. This paper focuses on the noninvasive temperature measurement of the intermediate product in ferrous or nonferrous metallurgical processes, such as molten salts in aluminum or rare-earth electrolyzer, molten alloy in melting furnace, and hot-rolled steel plates in the continuous casting process [1–5]. For such melts, as in common, there is often a need for temperature detection ranging from 200 to 1500 °C, while the real-time response sensitivity is less than 30 °C. In addition, since metallurgical processes are often accompanied by dusty, misty, toxic, and corrosive environments, those unfavorable factors are seriously corroded to the traditional invasive temperature sensor. For instance, in the high temperature of the continuous casting process, contact instruments can degrade with time. If the environment temperature is above the material limits, it would disintegrate completely.

*Corresponding author, E-mail: gzlff@126.com

Furthermore, the temperature of moving objects cannot be detected by contact temperature measurement. Thus, traditional invasive temperature measurement is no longer fully applicable.

When comparing traditional invasive temperature measurement with noninvasive measurement, the latter has received special attention in the last years, since it offers several outstanding advantages over its invasive counterparts. Among other characteristics, it can be highlighted that the instant response to temperature change, large measurement range, ability to measure the temperature of moving objects, and resistance in hazardous environments due to remote measurement make this technology suitable to be used in severe conditions, such as molten salt, molten matte, molten slag, and metal melts in metallurgical process.

Currently, several sensors for optical noninvasive temperature measurement have been reported, based on different sensing techniques, including radiation thermometry and computer vision-based measurement. In essence, both of them realize temperature detection by detecting light of different wavelengths in the radiant energy emitted by the measured object. The difference is that computer vision maps the light radiated by the object into the color and brightness of the pixel through the CCD sensor, which can apply a variety of image processing techniques and greatly expands the scope of radiation temperature measurement.

This paper is structured in the following sections: Following this introductory section (Sect. 1), a brief description of optical noninvasive temperature measurement is presented (Sect. 2). Radiation thermometers and computer vision-based measurement are described in detail, respectively (Sects. 3, 4). The final remarks of this review are summarized in Sect. 5, and a prospect of optical noncontact temperature measurement technology is placed in Sect. 6.

2. Optical Noninvasive Temperature Measurement

As mentioned above, the special occasion and requirement of high-temperature melts measurement determine that it can only be applied by using optical temperature sensors. Currently, optical temperature measurement (also called noncontact temperature measurement) for molten melts in a metallurgical process can be mainly divided into two categories. One temperature measurement is based on radiation thermometry [3–7], while the other temperature measurement is based on computer vision [8–19], which applies digital image processing technology to build a soft sensor model of temperature measurement. Both categories are discussed in detail below separately. It is important to point out that acoustic tomography (AT) [20–22] and laser radar measurements [23–25], also as optical temperature measurement technology, are difficult to deploy in the temperature measurement of molten melts, so those measurements are beyond our discussion. A truncated classification diagram of optical temperature measurement can be seen in Fig. 1.

2.1. Radiation Thermometry-Based Measurement

Entire material above zero kelvin emits infrared radiation. An optical thermometer, also known a as radiation thermometer, is applied to measure the temperature of a target according to the achievable level of thermal radiance emissions [26]. The technology is a noncontact, online, and safe surface temperature measurement. With appropriate traceable calibration [27], temperature measurement systems dependent on thermal radiation in the infrared spectrum are valid in the ranges from 50 to 6000 K. In the class variously present temperature real-time detecting methods, radiation thermometry has an irreplaceable status in temperature detection for the metallurgical process. It meets the demand of temperature measurement in the following cases while other methods may not fulfill needs [28]:

(1) Targets with fast speed.
(2) Rather tiny targets.
(3) Targets with poor heat conductivity or low heat capacity.
(4) Targets with shiftily altered temperature.
(5) Targets for which stereoscopic temperature fields need to be decided.
(6) Targets with extremely high temperatures.
(7) Situation where contact temperature measurement could not be deployed.

2.2. Computer Vision-Based Measurement

The temperature measurement method built on computer vision is an excellent optical measurement method. This method depends on CCD (charge-coupled device) to achieve images from the measured target and then processes the digital image with dedicated algorithms.

The CCD outputs analog level of three primary colors signals, consisting of red, green, and blue [29]. The image acquisition card performs the analog-to-digital conversion and delivers the image to the computer. After proper processing, a thermal radiation digital image of the measured object surface can be obtained. The digital image is composed of matrix pixels, and each pixel contains three numerical RGB values. According to the spectral response characteristic curve and the photoelectric conversion characteristic [30], it can be deduced that there is a one-to-one correspondence between the RGB value and the

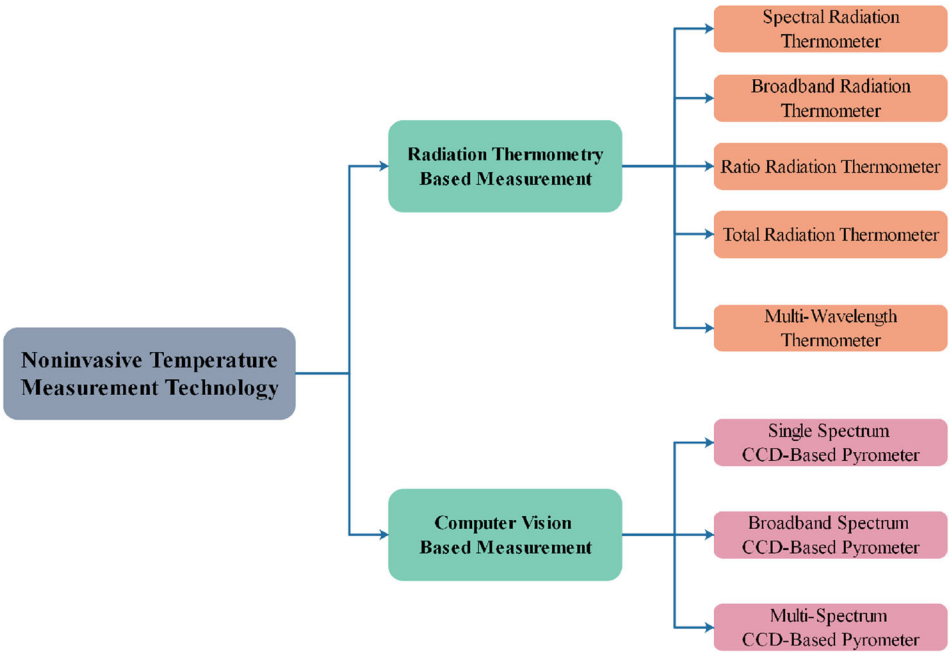

Fig. 1 Classification diagram of optical temperature measurement

spectral radiance in the particular spectral response band. The temperature field on the surface of the target can be determined from the output RGB value and corresponding temperature measurement algorithm.

Computer vision-based measurement has the advantages of low cost, convenience, simple operation, real-time measurement, and high efficiency compared to other methods. It has been applied more and more widely in practical production and scientific research. Therefore, exploring the mathematical model between the target temperature and the response of the CCD-based pyrometer is of great significance for the application [31].

3. Radiation Thermometers

3.1. General Structure and Characteristics

The general structure of a radiation thermometer, together with a standard deployed situation, is illustrated in Fig. 2. A set of optical components, including lens and aperture stop, displayed the measured target onto the field stop, which is located before the detector and both of them are put in a temperature-regulated detector housing. The fixed angle along with the detected area of the target (measurement field/field of view) is determined by not only the aperture stop but also the field stop [28, 32]. For commonly used radiation thermometers, a spectral filter acting as a band-pass filter is deployed to decrease the wavelength energy of the radiation arriving at the sensor. The band-pass filter is always deployed before the detector and regarded as the gate of the detector housing [28].

In actual application, several physical properties of radiation thermometers affected measurement results need to be considered carefully, including lens focus, quality of detector, and even the material of the optical system. Although radiation thermometers perform with recommended measuring distance that thermometer producers offer help to optimize the accuracy of radiation measurement, the most significant factor that influences the result of radiation thermometers' detection mainly depends on the optimization of the optical system and the radiation detector. When a radiation thermometer operates in a situation, the radiation temperature measurement area of the target is decided by the set length of lens focus. Another factor that determines the accuracy of radiation thermometers is the material of optical glass, which acts as the infrared-transparent components. Usually speaking, radiation thermometers applied in metallurgical process temperature measurement are always equipped with a rather sophisticated optical system, which consists of polarizers, prisms, beam splitters, or a combination of these. According to the varied focus length range of the radiation, a thermometer operates, and an optical lens could be made of different materials, such as zinc sulfide, zinc selenide, and fluorides. In low-cost radiation thermometers, particularly, plastic is often used in optical components [5, 28, 33].

Radiation thermometers do not detect temperature directly. On the contrary, they measured emitted infrared energy of interest. Because infrared energy corresponded to a target as a function of not only the body temperature but also the emissivity on the surface, the radiation thermometer calculates the temperature results depending on

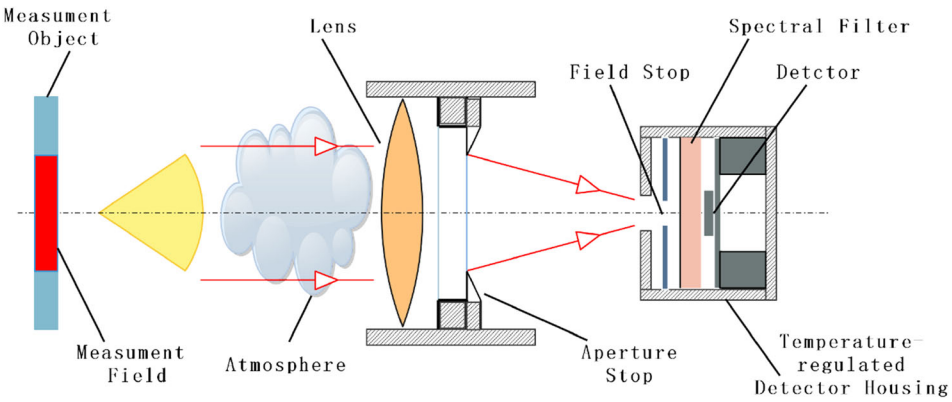

Fig. 2 Structure demonstration of a radiation thermometer

the assumption that the emissivity character is relatively stable to the measured object surface.

3.2. Classification of Radiation Thermometers

There are thousands of different radiation thermometers on the market, consisting of different types with a range of different models and specifications.

The essential difference between the main groups of radiation thermometers is, according to most research [3], the selection of the wavelength ranges detected. It leads to five kinds of classification, including spectral radiation thermometer, broadband radiation thermometer, ratio radiation thermometer, total radiation thermometer, and multi-wavelength thermometer. A diagram of the wavelength range for different types of radiation thermometers is demonstrated in Fig. 3 [5].

The common feature of those radiation thermometer sorts is that they are all calibrated according to the spectral radiance of a blackbody at given temperatures. A radiometer is simply an electro-optical system designed to measure radiant power [32]. Radiation thermometers are designed by the fact that the measured radiant power is proportional to the radiance of the target within a specified wavelength range.

3.2.1. Spectral Radiation Thermometer

Spectral radiation thermometers, also called single-color pyrometers, are by far the common types of radiation thermometers. They operate normally in a relatively short spectral range when the ratio of the spectrum width to the center frequency of the spectrum is less than 1 (it is called quasi-monochromatic light). Because spectral radiation

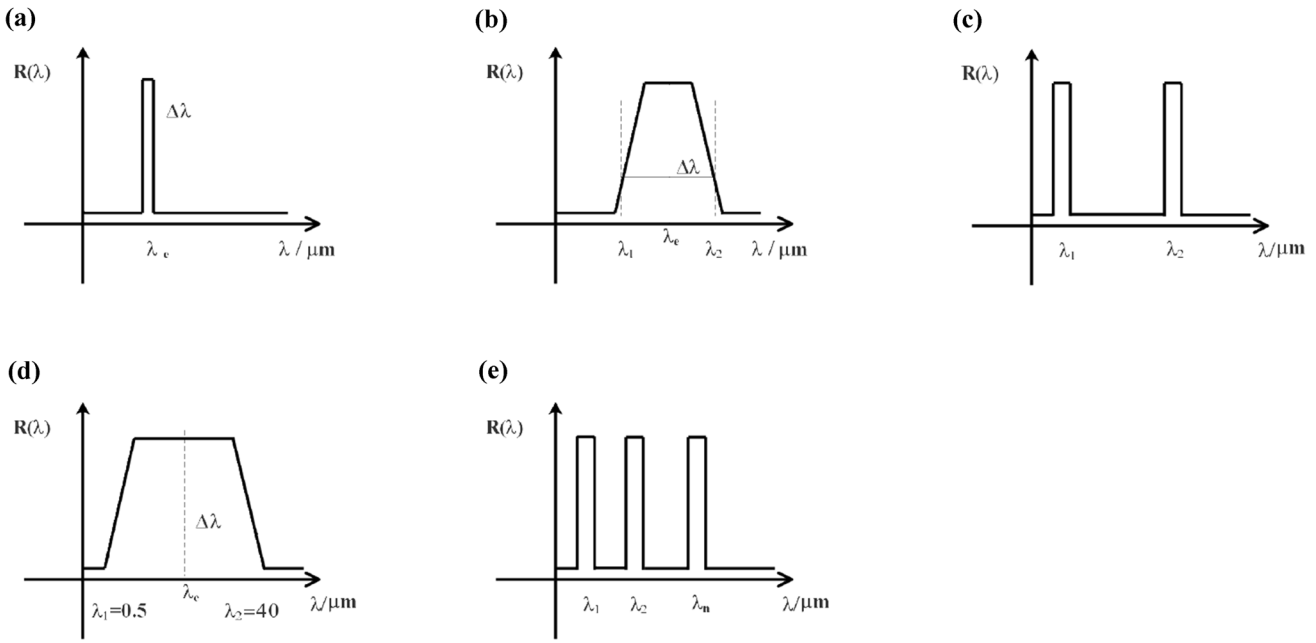

Fig. 3 Diagram of the wavelength range for different radiation thermometers: **a** spectral radiation thermometer, **b** broadband radiation thermometer, **c** ratio radiation thermometer, **d** total radiation thermometer, and **e** multi-wavelength radiation thermometer

thermometers receive the single-spectral radiation, they calculated an average temperature result from the target and background environment and they need to properly calibrate toward the hotter temperature. Without a doubt, the temperature measurement is also affected by emissivity floating, atmosphere abortion, and other factors. The oldest spectral radiation thermometer determines the object's temperature by comparing optical brightness in the visible (red) spectrum, which wavelength is at 0.65 μm by matching the lighten target to a hot "disappearing" flame. Particularly, a line scanner is a kind of brightness spot pyrometer equipped with a rotating mirror so that they can measure temperature along a line. By combining the temperature reading with the position of the rotating mirror, a thermal picture could be determined. Each successive swap along the line would measure the temperature of a new segment of a moving measured object. In metallurgical processes, this kind of thermometer is commonly used for measuring moving targets, or rotating objects such as impellers and grinding wheels [34].

Based on the assumption that the emissivity of the object is reasonably constant and known [35], the temperature of the object, which is related to the spectral emissivity, ε_λ, can be calculated according to Planck's law [5, 33], which is described in Eq. (1):

$$T = \frac{c_2}{\lambda \ln\left[\varepsilon_\lambda \left(\exp\left(\frac{c_2}{\lambda T_b}\right)\right) + 1\right]} \tag{1}$$

where c_2 is a constant with a value of 14,388 μm. K is the second constant of Planck's radiation law, and λ is the wavelength and temperature. T_b is the object temperature assuming it is a blackbody. The Wien approximation of Planck's Eq. is effective below 3000 K, which is generally permitted to use, as demonstrated in Eq. (2):

$$T = \left(\frac{1}{T_b} + \frac{\lambda}{c_2} \ln \varepsilon_\lambda\right) \tag{2}$$

The wavelength of a single-spectral infrared thermometer selection is relatively rather broad. It could be seen from the formula above that the measurement accuracy of the spectral radiation thermometer depends on the pre-knowledge of the target's surface actual emissivity value. However, that is not always achievable in actual applications. For example, in the process of continuous casting, external factors, such as steam, dust, atmospheric CO_2, and other participation media, would absorb the infrared radiation rather than allow it to pass undeterredly through the atmosphere, which adds the uncertainty of emissivity estimation. Thus, it would influence the temperature measurement accurateness of the slab. The sensitivity to emissivity variation and optical obstruction would be minimized by selecting the shortest practical wavelength [34]. Calro et al. carried out a semiempirical formula based on experiments to calculate the real emissivity of the target by the use of a single-color pyrometer [36]. The wavelength selection could always be an issue that confuses spectral radiation thermometer users. After comparing the measuring errors by spectral radiation thermometers, Huang showed that the optimum wavelength for high temperature measured would be near 1.0 μm or 1.6 μm [37].

Meanwhile, many researchers emphasized how to measure absolute infrared spectral radiation accurately against a complex background. Cassady et al. discovered that a 1% error associated with noise and calibration approximately led to an uncertainty in predicted temperature of less than 2%, while a spectral radiation thermometer had nearly a 5% uncertainty for all magnitudes of error [38]. In some cases, the errors might cause huge mistakes if it was regarded to be ignored. It was shown that deviation was up to 14.9% when the spectral radiance of the non-calibrated radiant source was measured compared to that of the standard source at 10 μm wavelength [39]. To suppress stray radiation, He et al. installed a shielding plate at the entrance of the optical system to optimize the measurement results, which showed the deviation between the standard source and the radiant source was limited to 1.42% at 10 μm wavelength. In addition, by the use of proper materials in radiation transformed components, spectral radiation measurement could be more accurate. YO et al. investigated the relationship between the material of high-temperature components and spectral emissivity in the application of direct thermal-to-electric power-conversion systems [40]. Sakuma studied the long-term spectral characteristics of the 0.9 mm spectral radiation thermometer by using a monochromator and a fixed-point blackbody. Studies have shown that some spectral radiation thermometers show a change in the center wavelength, but the short-term change is within an acceptable range.

In terms of applicability, spectral radiation thermometers are the most widely used radiation thermometers for radiance temperature measurements nowadays. They are generally used in low-temperature ranges and low-precision requirements. The wavelength center of its measurement may drift over time, which limits its long-term use in harsh industrial environments.

3.2.2. Broadband Radiation Thermometer

Broadband radiation thermometers are now the most popular used in many industrial applications. Broadband radiation thermometers monitor the intensity of infrared energy covered over a specific wavelength range. Broadband radiation thermometers always absorb the specific band spectral from the atmosphere. Among them, the main

effective wavelength that the broadband radiation thermometer received would change in terms of the target's surface temperature. The change of effective wavelength distribution results from alteration with temperature based on Wien's displacement law, as shown in Fig. 4. For broadband radiation temperature estimation, the equation below can be calculated by the use of numerical integration Eq. (3) [41]:

$$\int_{\lambda_1}^{\lambda_2} \frac{\lambda^{-5}}{\exp\left(\frac{c_2}{\lambda T_b}\right)-1} d\lambda = \int_{\lambda_1}^{\lambda_2} \frac{\varepsilon_\lambda \lambda^{-5}}{\exp\left(\frac{c_2}{\lambda T}\right)-1} d\lambda \quad (3)$$

where c_2 is the second constant of Planck's radiation law which has a value of 14,388 μm· K. λ_1 and λ_2 are the wavelength distribution range. T_b is the object temperature assuming it to be a blackbody. ε is the total emissivity.

Infrared imagers are real-time, long-distance, and optical measurement tools, and they are widely used in metallurgy industries. Those temperature results are specially visualized graphically on a screen, with various colors standing for corresponding temperatures. The magnitude of the signal value output by the thermal imager is proportional to the irradiance it received. Therefore, the intensity of the image color on display change proportionally with the irradiance received by the sensor, so that the temperature of the target could be imaged and measured. Customarily, a focal plane array (FPA) thermal imagers can detect radiation in short-wave (SWIR), medium-wave (MWIR), and long-wave (LWIR) bands, with wavelength windows of 1–2.5 μm, 3–5 μm, and 8–14 μm, respectively. Among them, the 3–5 μm and 8–12 μm broadband radiation thermometer operating wavelengths in the medium- and long-wave bands play a particularly wide role in practical applications. Because of its exceptionally strong radiation ability, the medium-wave infrared system is mainly used in aircraft, rockets, tanks, and other high-temperature weapons and equipment, while the long-wave infrared system is mainly used in low-temperature environments such as biological radiation.

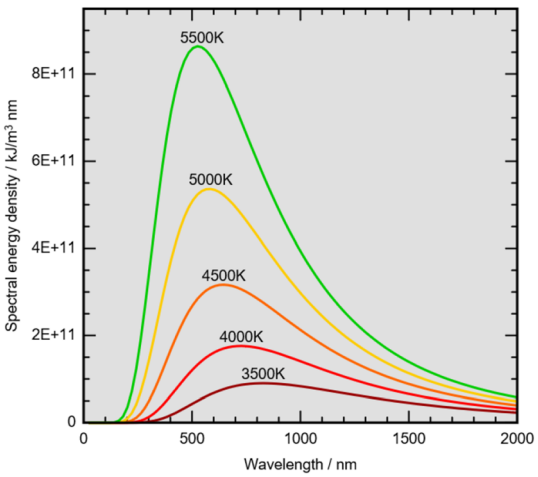

Fig. 4 Black-body radiation as a function of wavelength for various temperatures [42]

Noted from Eq. (3), the accuracy of the infrared thermal imager is affected by the factor of emissivity and some other relative factors. It is important to point out that even if by selecting the proper wavelength of broadband radiation thermometers which does not belong to atmospheric absorption bands, the achieved measurement uncertainties could not be controlled as low as that achieved with spectral radiation thermometers [28]. The angle of view and measuring distance is all relative to the measurements.

Recently, research focused on the error theory of infrared imagers has become popular. Shen et al. studied the effect of temperature and surface condition, respectively, on the deviation of emissivity and carried out a non-steady temperature field model for infrared thermal images in different emissivity situations [43]. Zhang et al. came up with a compensation algorithm, which was based on G–t standard curve, to get better temperature accuracy of the focal plane [44, 45]. Combining the advantages of both PSO and BPNN methods, Zhao et al. built a mathematical model to minimize the effect of ambient temperature disturbance on the temperature measurement accuracy of infrared thermal imager [46]. Through analysis of the impact of field angle and temperature measuring angle of the infrared thermal imager, Muniz et al. carried out and verified a compensation algorithm based on neural network and regression to eliminate the impact [47]. Zhang et al. explored the relationship between measuring distance and measurement deviation and then carried out a piecewise fitting to offset the deviation [48].

Aimed at the high-temperature melts measurement application of thermal imagers, Pan found impact from dust and vapor could not be ignored, particularly in the metallurgy process [49]. A compensation model also was carried out to compensate ate the result and experimental results had proven its effectiveness. Yang et al. developed a real-time heat transfer model for dynamic control in the process of continuous casting billets, and then it was calibrated by infrared imagers to online monitor the cutting tool's temperature during the whole milling process [50], Bagavathiappan et al. mapped the temperature distribution of the micro-end milling tool workpiece with thermal imagers [51]. It was observed that the measurement result of thermal imagers was affected by rotation speed significantly other than feed rate.

3.2.3. Ratio Radiation Thermometer

The ratio radiation thermometers, often called tpyrometerspyrometers, measure the ratio of radiation detected at

two nearby wavelengths (strictly, over two separate wavelength bands). The ratio result is not influenced by accurate emissivity caused by obstructions, because the ratio radiation thermometer absorbs both wavelengths equally. Therefore, ratio radiation thermometers are cables of amending for emissivity variation and viewing through vapor, dirt, and many various optical obstructions, which consist of dirty lenses particularly. Under this condition, the temperature is calculated by Eq. (4), in which Wien's displacement law is also applied [41]:

$$\frac{1}{T}-\frac{1}{T_{\mathrm{r}}}=\frac{\lambda_1\lambda_2}{c_2(\lambda_2-\lambda_1)}\ln\left(\frac{\varepsilon_{\lambda 1}}{\varepsilon_{\lambda 2}}\right) \tag{4}$$

where T_{r} is the ratio temperature. The T_{r} temperature is the temperature that is equal to a blackbody having the same ratio of spectral radiances at λ_1 and λ_2 wavelengths as the surface whose spectral emissivity values are $\varepsilon_{\lambda 1}$ and $\varepsilon_{\lambda 2}$, respectively.

The most significant feature for measurements with the ratio radiation thermometer is to regard the target's surface as a gray body, which means that the emissivity of each wavelength is identical. As a result, it is not necessary to have a priori knowledge of the target's surface emissivity characteristics before the ratio thermometer is deployed. Moreover, ratio thermometers could be applied reliably without being calibrated [52]. However, if the emissivity of the materials varies with wavelength, the measurements can cause large errors. In general, often the great advantage of the ratio radiation thermometer lies in the following three conditions:

(1) Exist window contamination, such as dust or smoke;
(2) Targets that are merely fractional filling the measurement window;
(3) Small target which is compared to the measurement window.

In the metallurgical environment, the influence of unaccounted external factors is inevitable, such as clouds or water vapor that randomly be distributed in the transmission area between a target and a radiation thermometer. A ratio thermometer could operate normally with an optical obstruction because both wavelengths are obstructed equally. For instance, ratio radiation with two selected wavebands centered in the 0.7 μm and 0.8 μm range would pass through the vapor without absorption while a thermometer filtered at 0.8 μm and 0.9 μm would lead to only minimal deviation. And the thermometer filtered at 0.7 μm and 1.1 μm would cause a relatively large deviation, the reason for which is that vapor absorbed much more infrared energy at wavelengths beyond 1 μm than at wavelengths shorter than 1 μm [34].

In this case, ratio radiation thermometers have a unique advantage over other radiation thermometers. It had been proved by Chernysheva et al. through simulation that dual-channel spectral ratio radiation thermometers offered more efficient and accurate measurement results than that spectral radiation thermometers [53]. For the common case of the unknown material thermo-optical properties, Hernandez et al. verified the use of a ratio thermometer to measure the temperatures of hot metals when the emissivity was unknown and for the commercially important case of specular surfaces by comparison of measurements made for tungsten, copper, and aluminum samples of various roughness, determined by a roughness gauge [54].

A ratio radiation thermometer measures the radiance ratio of the target at two selected wavelengths, thereby eliminating the influence of the emissivity of the material and obtaining its true temperature. This method is more effective for gray-body materials, but it will cause larger errors for general non-gray-body materials. In the actual application of ratio radiation thermometer, factors such as atmospheric environment should be considered to select the appropriate band. The principle is to select a smaller wavelength under the premise of detectable intensity and make the two wavelengths as close as possible. Generally speaking, the temperature measured by a ratio radiation thermometer is closer to the real temperature than the spectral radiation thermometer and total radiation thermometer.

3.2.4. *Total Radiation Thermometer*

Total radiation thermometers receive almost the whole thermal radiation to determine the temperature of the target commonly instead of using a band-pass filter. The radiant spectrum arrived at the thermometer is huge because the bandwidth of the whole spectrum is relatively wide. Nevertheless, only in the environment of a vacuum or with an inert gas could the high accurate calibration of total radiation thermometers be achievable in such extreme constant atmospheric situations. The metallurgical application of total radiation thermometers is almost unable to deploy because the accuracy of total radiation thermometers was sensible to the surrounding environment [28]. Under ideal conditions, the temperature of total radiation thermometers is then estimated as an average of the whole radiation spectrum reaching the thermometer. Thus, the temperature is described as Eq. (5):

$$T=\sqrt[4]{\frac{T_b^4}{\varepsilon}} \tag{5}$$

where ε is the total emissivity.

Total radiation thermometers receive the whole spectrum, so there is no way to reduce errors by optimizing the spectrum. This problem must be solved by optimizing the hardware. In 1996, Martin et al. adopted a new and

accurate method with an electrical substitution cryogenic radiometer to measure thermodynamic temperature, which was used in the temperature range from about − 140 to 100 °C [55, 56]. The results showed that the values of uncertainties were below 0.8 °C. One typical type of total radiation thermometer is called a gold-cup pyrometer [57–62]. A gold-plated hemisphere is placed on the surface of interest and serves to form a blackbody collecting nearly all the radiation emitting from the surface. When the hemisphere is placed against the surface to be measured, it forms a blackbody cavity so that the radiation passing through the window is unrelated to the emissivity of the surface.

A total radiation thermometer is designed based on Stefan–Boltzmann's law, and its advantage is the ability to receive radiation. But its shortcomings are also obvious. Because the intermediate medium in the environment can absorb radiant energy, the radiant energy received by the total radiation thermometer is reduced, resulting in errors caused by low indications. Under normal conditions, the energy absorbed by the air is very small. However, it will increase with the increase of the water vapor and CO_2 content in the air. To reduce this error, the distance between the measured object and the total radiation thermometer should preferably not exceed 2 m.

3.2.5. *Multi-wavelength Thermometer*

It should be pointed out that the abovementioned spectral radiation thermometer (including broadband radiation thermometer), ratio radiation thermometer, and total radiation thermometer do not measure the actual temperature of the object, but are the brightness temperature, color temperature, and radiation temperature, respectively. To determine the true temperature of the object, the emissivity must be calibrated. The emissivity of an object is often related to different factors such as the material, temperature, radiation wavelength, and surface state of the object, which inevitably brought difficulties to the correction. The multi-wavelength thermometer is a continuation of this idea of which ratio radiation thermometer operated. A multi-wavelength thermometer measured infrared energy at three or more wavelengths and determined the object's temperature based on the specific algorithm which is designed specifically for this occasion. On this occasion, it is commonly regarded that the determination of the changeable emissivity could be resolved by describing the emissivity as the function of multiple wavelengths [5, 28, 33].

The complexity of the thermometers and the temperature transformed algorithms changed according to the actual deployment need. This kind of thermometer is always adopted for materials, and applications where traditional broadband or ratio thermometers are inapplicable. The output signal S of the n channel from a multi-wavelength thermometer can be expressed as Eq. (6).

$$S_i = \frac{K_i \varepsilon(\lambda_i, T) c_i \lambda^{-5}}{\exp\left(\frac{c_2}{\lambda_i} - 1\right)} \tag{6}$$

where K_i is the geometric factor of the i channel, which is related to the spectral response of the detector and the optical transmittance of the optical device. It can be obtained by calibration.

There are n equations in total and $n + 1$ variables, so the equations cannot be solved directly. An extra function of emissivity and wavelength is needed to form a certain relationship with the wavelength, so that the number of variables in the system of equations is less than or equal to n and then the true temperature and spectral emissivity of the target could be calculated by solving the equations. Typically, this additional equation is based on the properties of the designed multi-wavelength radiometer, and how to construct this equation is the focus of the study of multi-wavelength thermometry. In 1981, Barker et al. firstly created a six-wavelength thermometer [63], of which the working wavelength was from 0.75 to 1.6 μm with a temperature measurement range of 726.85 to 1326.85 °C. In 2001, Dai et al. successfully developed an eight-wavelength thermometer that simultaneously measured the true temperature of the target and the spectral emissivity. Based on the emissivity hypothesis model, the true temperature of the rocket's plume was detected [64].

The wavelength selection of multi-wavelength thermometers depended on the actual application. Xue et al. applied a technique in which a multi-wavelength pyrometer was used to measure a sample temperature with its short wavelength based on the reflectivity measurement and then to obtain the normal spectral emissivity at longer wavelengths [65]. Wang et al. designed an experimental apparatus to measure the emissivity of a steel surface in both vacuum and oxidation atmosphere [66]. The surface temperature fluctuation of casting billets was reduced from ± 20.7 to ± 2.8 °C based on multi-wavelength thermometry. For the temperature range of 1426.85 to 2726.85 °C, typical of electrode surfaces in high-power electric propulsion thrusters, Leonard et al. proposed an east-squares multi-color pyrometer method and the results proved that the method could achieve higher accuracy [38].

Multi-wavelength thermometers are more widely used than total radiation thermometers. Typical applications include solid rocket motor tail flame temperature measurement, explosive temperature measurement, and smelted metals that require high-temperature accuracy. This method is currently the most accurate in radiation temperature measurement, but its disadvantage is that the

physical structure is complex, and the multi-wavelength true temperature construction algorithm and effective wavelength calibration algorithm are still quite difficult.

3.3. Selection Principle of Radiation Thermometer

Generally, choosing a radiation thermometer requires careful consideration. Firstly, the wavelength selection of the radiation thermometer is perhaps the most important optimization consideration for radiation measurement accuracy. Wavelength selection of radiation thermometer not only significantly impacts the ability to measure emitted energy from objects through certain intervening media, such as vapor or smoke, but also dramatically influences the effect to measure low emissivity targets such as glass. Besides, each radiation thermometer uses a different wavelength range and has a corresponding optimal temperature range. Table 1 reveals the effective wavelength distribution at different temperatures for the spectral ranges of several classical broadband radiation thermometers [5, 28, 33]. Once used in an application beyond this range, it will have a more or less impact on the accuracy of its temperature measurement. For example, the temperature measurement environment of infrared thermometers used in the medical field is very different from that of the metallurgical industry.

Secondly, it requires consideration of the distance between the radiation thermometer and the object to be measured. Selecting the optimal distance for temperature measurement will be more conducive to obtaining accurate temperature data. The determination of this distance should comprehensively consider the factors affecting the size of the measured object and the personal safety factors of the measuring personnel. While measuring the temperature, it must be ensured that the distance will not damage the radiation thermometer itself. Finally, attention should be paid to the influence of the temperature measurement environment. If the temperature measurement site has large influencing factors such as dust, the environment needs to be cleaned up in advance to create a temperature measurement environment without objective interference and obstruction.

Thirdly, it is necessary to know another key parameter of the object, namely the emissivity, to calculate the true temperature of the target. As we all know, the material emissivity of an object is not only related to the composition of the object, its surface state, and temperature. It is easy to change with the surface condition, and it is not easy to measure online. To measure the true temperature of the target surface, the most accurate method is to use a thermometer with multiple wavelengths to obtain the relationship between emissivity and wavelength. A multi-wavelength thermometer sets a pyrometer as an instrument with more than two spectral channels. It obtains the true temperature of the measured target by processing the brightness temperature information of the measured target collected at multiple wavelengths, combined with the true temperature construction method.

Table 1 Effective wavelengths at various radiation temperatures for the spectral ranges of a spectral radiation thermometer at 0.65 mm and typical industrial band radiation thermometers [28]

Temperature (°C)	Wavelength (μm)					
	From 0.65 to 0.65	From 0.7 to 1.2	From 1.1 to 1.7	From 2.0 to 2.5	From 4.5 to 5.5	From 8.0 to 14.0
− 100	–	–	–	–	5.16	11.43
0	–	–	–	–	5.07	10.71
100	–	–	–	2.34	5.03	10.36
200	–	–	1.57	2.31	5.00	10.16
300	–	–	1.57	2.30	4.99	10.04
400	–	1.13	1.55	2.28	4.97	9.95
500	–	1.11	1.53	2.27	4.96	9.89
600	0.65	1.10	1.51	2.26	4.95	9.84
800	0.65	1.08	1.47	2.25	4.94	9.78
1000	0.65	1.05	1.44	2.24	4.94	9.73
1200	0.65	1.03	1.42	2.23	4.93	9.70
1400	0.65	1.01	1.40	2.23	4.93	9.68
1600	0.65	1.00	1.39	2.23	4.93	9.66
1800	0.65	0.98	1.38	2.22	4.92	9.64
2000	0.65	0.97	1.37	2.22	4.92	9.63
2500	0.65	0.94	1.35	2.22	4.92	9.61
3000	0.65	0.92	1.34	2.21	4.91	9.60

Table 2 Part characteristics of typical commercial spectral, broadband, and ratio thermometers [28]

	Wavelength (μm)								
	1.1	2.4	3.5	7.5–8.2	8–10	8–14	0.8/1.1	0.95/1.05	1/1.5
Temperature range (°C)	450–3000	50–2500	0–2500	0–2500	0–1000	− 100 to 1000	600–3000	600–3000	500–3000
Response time (ms)	1	1.5	1.5	5	5	5	1	10	2
Types of detectors used	Si	PbS, Pyro, TP	PbSe, Pyro, TP	Pyro	Pyro, TP	Pyro, TP	Si/Si	Si/Si	Si/Ge, Si/InGaAs
Typical applications	Metals, molten glass, ceramics, semiconductors	Metals, molten glass	Metals, ceramics, hot–melt adhesives	Glass surface, ceramics	Plastics, non–metals, ceramics	Organic materials, lacquers, rubber, oils	Molten metal, graphite, molten glass	Molten metal, graphite, molten glass	Molten metal, graphite, molten glass

In conclusion, Table 2 lists the various characteristics of commercially available typical radiation thermometers, including temperature range, response time, detector materials, etc.

4. Computer Vision-Based Pyrometers

4.1. General Structure and Characteristics

With the availability of low-cost CCD (charge-coupled device) colorful sensors and recent advances in digital image processing techniques, computer vision-based pyrometers, of which a CCD camera is a core component, have been developed for temperature measurement in various industrial fields. As computer vision-based pyrometers always adopt a CCD as a sensor, they are also called CCD-based pyrometers for short.

Compared with radiation thermometers, computer vision-based pyrometers mainly receive visible light (0.38–0.74 μm) or near-infrared light (0.75–1.1 μm), while radiation thermometers receive a wider spectrum span, including infrared light, ultraviolet light, and visible light, from 0.5 to 40 μm. Currently, the spectral response of commercial computer vision-based pyrometers can be extended to 1.1 μm, which can be used to measure temperatures higher than 1000 K. Figure 5 shows a relative individual spectral response of a CCD sensor for the red (R), green (G), and blue (B) channels, respectively, taking into account the infrared filter included in the RETIGA 1300C camera [67].

From the spectral response characteristics and photoelectric conversion characteristics of the CCD, it can be known that the output value of the CCD reflects the brightness and the radiated light chromaticity information on the surface of the measured target, and the radiated light information of the object has a specific relationship with

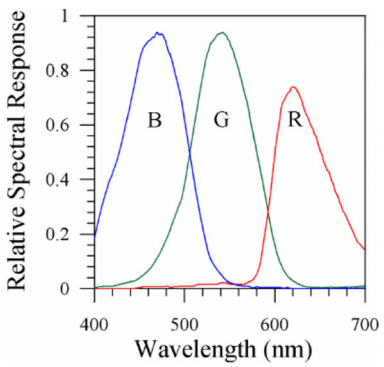

Fig. 5 Relative spectral response of the ICX085AK CCD sensor for the red (R), green (G), and blue (B) channels, taking into account the infrared filter included in the RETIGA 1300C camera

the object temperature. According to the thermal radiation theory, the surface temperature field of the radiator could be calculated from the output of the CCD image information. For CCD-based pyrometers, Wien's Law lay a theoretical foundation for CCD temperature measurement. Since the emissivity is difficult to obtain, to avoid calculating the emissivity directly, the radiant energy measured in the R channel and G channel of the CCD sensor is used to calculate the temperature:

$$T = \frac{c_2\left(\frac{1}{\lambda_g} - \frac{1}{\lambda_r}\right)}{\ln\frac{M_R}{M_G} + K + 5\ln\frac{\lambda_r}{\lambda_g}} \tag{7}$$

where λ_r and λ_g are the wavelengths of the R and G channels of the CCD sensor, M_R and M_G are the luminance response values of R and G channels, and K is the correction factor related to camera parameters, exposure time, and emissivity of the object, which can be calibrated experimentally. Therefore, as a photoelectric conversion device, it can be used to achieve noncontact temperature measurement. In addition to the advantages of traditional radiation temperature measurement, this temperature measurement method also has the following outstanding advantages [19]:

(1) The measurement results are less affected by the emissivity of the measured target and the selective absorption of various media in the way of radiation.
(2) The measurement results are less affected by the temperature measurement environment with strong electromagnetic interference and toxic gases.
(3) The measurement results can give the surface temperature gradient field of the measured target and realize the pseudo-color display of the surface temperature gradient field on a screen.
(4) The measurement results are convenient for long-distance transmission of measurement data via the network to realize remote monitoring and data sharing.

The basic principle of temperature field measurement with the sensor of a planar CCD is shown in Fig. 6. The optical system projects the optical radiated information of the target onto the photosensitive element at the surface of the CCD to form an optical image. The CCD converts the optical image on the surface of the photosensitive element into a proportional electric charge corresponding to the light intensity under the control of the electronic shutter. The accumulated electric charge is driven into thermal images at the output of the CCD. The magnitude of each discrete voltage signal in the video signal corresponds to the intensity of the radiation energy achieved by the photosensitive cell, and the timing of signal output corresponds to the spatial arrangement order of the position of the CCD photosensitive cell. The video signal from the CCD output is then processed by the video acquisition and signal processing circuit and then handed over to the computer for further processing.

4.2. Classification of CCD-Based Pyrometers

The CCD-based temperature measurement technology is still under research, and there is no unified classification standard. According to the number of spectra used in CCD-based pyrometers, this paper classifies CCD-based pyrometers into three categories: single spectrum, broadband spectrum, and multi-spectrum. The structural difference between those three CCD-based pyrometers remains in whether to add a beam splitter in front of the CCD-based pyrometers lens. The difference between them mainly lies in the device, temperature range, or operating band used for temperature measurement. The research progress is introduced as follows.

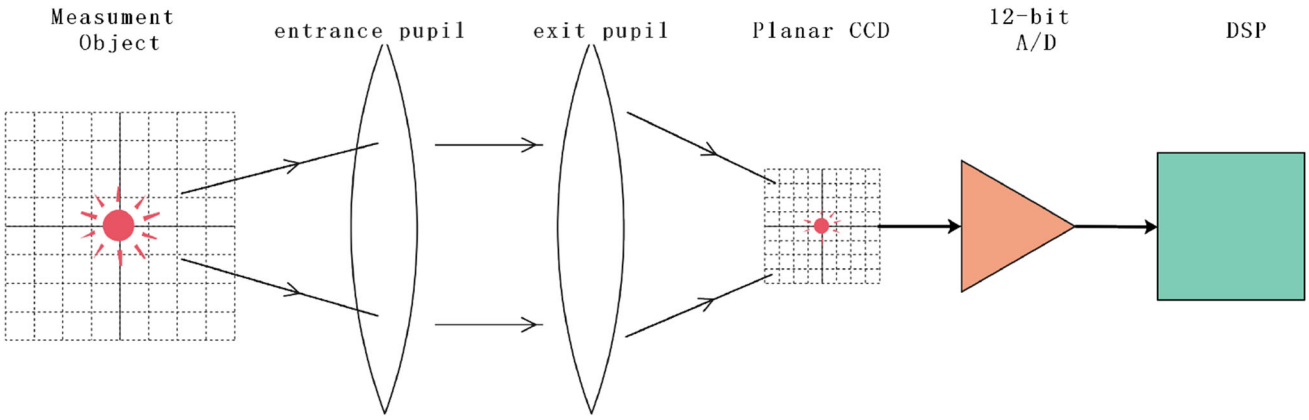

Fig. 6 principal of temperature field measurement with the sensor of a planar CCD

4.2.1. Single-Spectrum CCD-Based Pyrometer

The physical structure of the single-spectrum CCD-based pyrometers is similar to that of the broadband spectrum CCD-based pyrometers, except that the neutral attenuation plate is replaced by a narrow band-pass filter so that the influence of air absorption can be avoided.

In 1993, Keanini et al. used single-spectrum CCD-based pyrometers to test and study the time-varying temperature field on the solution surface, but the result did not turn out to be ideal [68]. In 2003, Suterer et al. tested a CCD-based pyrometer to measure a single spectrum emitted from the surface of an object which was approximately regarded as a blackbody, and the accuracy was extremely high [69]. By adding a filter in front of the CCD cameras to improve the sensitivity of the temperature measurement, Renier et al. invented a type of strengthened CCD-based pyrometers which were used in the steel industry [70]. Assuming that the flame structure was symmetric, Lu et al. tried to apply the Radon transform theory to rebuild the dimensional temperature field of the flame image acquired by a single-spectrum CCD-based pyrometer in the laboratory [71]. An algorithm for measuring the temperature gradient field of a monochrome image based on a reference point was proposed by Zhou et al. [72]. This method was adopted to calibrate the magnitude of the CCD output signal to the corresponding point temperature, which was measured by thermometers. Although this method was relatively simple, the specific position of the reference point was difficult to determine, which makes it difficult to apply in actual measurement.

4.2.2. Broadband Spectrum CCD-Based Pyrometer

Similar to single-spectrum CCD-based pyrometers, broadband spectrum CCD-based pyrometers also used commercial CCDs to perform multi-point calibration between temperature ranges and a certain set of optical parameters with a blackbody furnace. The broadband spectrum CCD-based pyrometers do not need to be spectroscopic, as long as a neutral attenuation plate or filter is installed on the optical lens of CCD cameras. Then they are calibrated by a standard source so that measurement of high temperature can be achieved.

As early as 1985, the HACCS-3000 system invented by Hitachi was designed to obtain the flame temperature distribution information with the use of flame image recognition technology. In 1990, Shimoda et al. deployed broadband spectrum CCD-based cameras which had a flat sensitivity in wavelengths from 400 to 1000 nm on the 175 MW unit of Sendai Power Station [73]. Assumed that the target under test had blackbody characteristics, Rank et al. (2005) developed a general broadband spectrum pyrometer with an effective wavelength range from 0.4 to 0.9 μm using ordinary commercial CCDs. In 2017, Zhang et al. established a radiation temperature measurement model for a narrow band-pass spectrum CCD-based pyrometer system, and the nonuniformity and photometric distortion caused by CCD arrays in the optical system were analyzed in detail and compensated [18].

4.2.3. Multi-spectrum CCD-Based Pyrometer

The multi-spectral CCD-based pyrometer was invented to overcome the impact of target emissivity on the temperature measurement results. Two or more spectra are used to collect two or more single-spectral images, and then these images are processed by algorithms to obtain the target true temperature field temperature distribution. Many researchers are committed to the development of multi-spectral image temperature measurement technology and have proposed various solutions. In conclusion, the existing multi-spectrum CCD-based pyrometers are based on either multiple single-spectrum CCD cameras (including colorful cameras) or multiple filters.

Paul et al. developed an advanced three-color pyrometer that depended on plenoptic imaging technology [74]. Three band-pass filters set before a CCD camera lens allowed separate 2D images to be obtained on a single image sensor at three different and adjustable wavelengths. Images were obtained of different blackbody or gray-body targets and results proved that the instrument could measure temperature with accuracy and precision of 10 K between 826.85 and 1076.85 °C. Meriaudeau et al. built a multi-spectral temperature measurement system based on dual CCDs and narrow band-pass filters to measure the temperature field distribution on metal surfaces in 2007 [70]. The middle wavelengths of the two filters were 750 and 950 nm, respectively. Cheng et al. proposed a method for measuring the temperature of the three primary colors. The principle combined the blackbody radiation Planck's law and the three primary color theories of human eye color perception in colorimetry and used the color matching curve of the human eye to finally establish an equation set between the radiation energy and the output data.

Since a color CCD and its built-in mosaic filter could easily obtain the brightness information of triple primary colors, such as R, G, and B, without the need for an additional spectroscopic system, a color CCD-based pyrometer had attracted much attention. In 2008, Lu et al. announced a three-color temperature measurement algorithm based on a color CCD camera [75, 76]. The results showed that the flame temperature measured by this instrument was consistent with the temperature measured by the thermocouple. A temperature measurement [11, 48, 49] and compensation methods are proposed by

Jiang et al. based on computer vision. Industrial experiments and applications demonstrated the proposed method, and the infrared computer vision system could realize the continuous accurate measurement of the molten iron temperature at the tap hole and provide reliable temperature data for operators.

4.3. Applications of Computer Vision-Based Pyrometers

The current CCD-based image temperature measurement technology has attracted extensive attention from experts and scholars due to its advantages, such as noncontact temperature measurement, rapid response, low cost, high resolution, real-time monitoring of the full temperature field, and convenient digitization and image processing. However, most of the research is limited to laboratory research using commercial monochrome or multi-color image cameras, and there are few specialized CCD-based measuring instrument products. The main reasons are as follows:

(1) The core component of a computer vision-based pyrometer is a CCD camera, originally designed to meet the general public's needs for recording video. Its temperature measurement range is narrow, and it is difficult to meet the needs of large-span temperature field measurement [19, 77].
(2) Due to the inevitable distortion and vignetting of the optical lens, and the inconsistency of the intensity response between the CCD pixels, the CCD camera will produce inconsistencies in-plane accuracy when used for temperature measurement. Especially when the field of view angle is large, the measurement results of the average temperature field of different pixels will produce large differences [78–82].
(3) Existed computer vision-based pyrometers are calibrated at a fixed distance and optical parameters. In many cases of the actual industrial situation, the distance from the measured target to the temperature measurement system is inconsistent with the calibration distance, and it requires parameters such as aperture and focal length to be appropriately adjusted again. Sometimes small changes in these geometric and optical parameters will cause large measurement errors [83–87].
(4) Although a CCD-based pyrometer has a simple structure and low cost, the dynamic range of pixels corresponding to each wavelength cannot be fully utilized at the same time. Only one wavelength corresponding to the dynamic range of pixels can be sufficiently used [88–93].
(5) Existed image-based cameras cannot embed user programs inside and can only output their video to a computer for algorithm processing, which greatly limits the performance of the temperature measurement device [93–97].
(6) The existed CCD image temperature measuring device cannot eliminate the dark current noise well, so the measurement accuracy of the low-temperature section is much lower than that of the high-temperature section [97–101].

5. Conclusion

5.1. Comparison Between Optical Noninvasive Temperature Measurement

Optical temperature measurement technology can be mainly divided into two categories according to the working principle, which are radiation thermometers and computer vision-based pyrometers. Most of the details have been illustrated above. Here a parallel comparison among them was performed, focusing on their parameter differences (Table 3).

5.2. Discussion on Measurement Uncertainty

The uncertainty remains existing in both optical noninvasive temperature measurements, but each comes from different sources. As for radiation thermometers, the emissivity of material surface and the absorption of transmission media are always the main problems needed to be solved. Those problems could be partly solved by using ratio radiation thermometers or multi-wavelength thermometers. In particular, atmospheric absorption could be minimized or even eliminated by the optimization of wavelength selection. When it comes to computer vision-based pyrometers, the target temperature mainly depends on the intensity of its luminous brightness captured by the CCD sensor. The uncertainty mainly comes from the resolution capability of the CCD sensor and the causal relationship between the temperature of the target and its brightness. Therefore, choosing a CCD sensor with high sensitivity is beneficial to reduce measurement errors.

6. Current and Future Developments

With no doubt, there are more and more researches and applications of optical temperature measurement technology. Generally speaking, radiation thermometers would be

Table 3 Parallel comparison between radiation thermometers and computer vision-based pyrometers

	Radiation thermometers	Computer vision-based pyrometers
Target requirements	Higher than absolute zero	Hot enough and causes a glow
Spectral range/(μm)	Mainly from 0.65–14	Mainly from 0.5–40
Measurement upper limit/(K)	Almost unlimited	Reached 3000K in literature
Temperature range	Mainly from − 100 to 3000 °C	Determined by CCD sensors
Temperature resolution	± 0.1 K was easily achieved	10 K achieved in the lab
Measurement precision	0.1 K or more accurate	Determined by CCD sensors
Measurement accuracy	High	Relative low
Response speed	Instant	Instant
Measurement field	Point	Plane
Typical applications	Industrial temperature measurement, such as molten metal, graphite, etc.	Mainly still in the research stage, commercial products were rare

used more widely in metals, molten glass, ceramics, semiconductors, etc.

Among them, the multi-wavelength thermometer is theoretically the most accurate in this article. It solves the problem of the emissivity model in the ratio method while retaining some of its advantages of that. Thereby, it is widely used on many occasions. However, the multi-wavelength temperature measurement method still has shortcomings. First of all, the emissivity function obtained by fitting may not be consistent with the actual situation. There are many unavoidable factors, such as whether the emissivity function model conforms to the actual situation, the size of the measurement error, and the fitting method. Due to the complexity of the fitting process, the error result is not easy to estimate. Researchers found that within a certain wavelength range, increasing the number of wavelengths will increase the error of fitting temperature. When the assumed emissivity model does not match the actual one, the fitting temperature error will also increase with the increase in the number of wavelengths. Besides, complex spectroscopy and detection systems increase the technical difficulty, uncertainty, and cost of temperature measurement, which limits the application of the multi-wavelength method. Moreover, limited by the working principle, most of the current radiation temperature measurement methods, except for the CCD-based radiation imagers to obtain two-dimensional radiation fields, are still limited to point measurements. The three-dimensional temperature field cannot be directly measured because no radiation thermometer can measure the three-dimensional radiation field. At present, the three-dimensional radiation field can only be reconstructed from multiple sets of two-dimensional radiation measurement results, and then the three-dimensional temperature field can be obtained from the three-dimensional radiation field. At present, the most researched is computed tomography based on various optical principles.

With the continuous development of computer and electronic technology, the monitoring method of high-temperature field based on a CCD-based pyrometer has attracted wide attention. This method has the advantages of noncontact measurement, rapid response, low cost, high resolution, real-time monitoring of the entire temperature field, and high-speed image processing. However, the spectral response of the CCD sensor itself is difficult to establish a strict mathematical model with the temperature of the target, and the measurement accuracy of the CCD-based pyrometer is relatively low, which is the main reason limits the popularization of CCD-based measurement technology. In addition, the CCD camera's exposure time, focal length, aperture, gain, brightness, etc., all have a great influence on imaging. Different application scenarios even use the same CCD-based pyrometer may cause huge differences in measurement results. Although the above facts determine that a CCD-based pyrometer can only be used specifically for applications, it can be used as a proprietary three-dimensional temperature field temperature measuring instrument and still plays an important and irreplaceable role. For example, the "HIACS-MULTI" system developed by Hitachi Research Institute in Japan for monitoring the flame temperature field of power plants uses CCD optical image sensors to identify furnace flames. It is worth noting that the rapid development of artificial intelligence technology in recent years has a good ability to classify and recognize images. Especially for the high-temperature melt in the metallurgical process, because the accuracy of measuring temperature is not high, but it may be necessary to measure the temperature of two-dimensional or even three-dimensional temperature field, the new temperature measurement technology combining CCD-based pyrometer and AI is suitable for this kind of occasions. In addition,

some dynamic feature extraction algorithms in artificial intelligence show great applicability to flame features accompanied by melts. Computer vision-based pyrometers have gained more interest from researchers due to their low cost and simple structure, and they are expected to be commercially available.

Funding Project supported by Jiangxi Ionic Rare Earth Resources Green Development and High-value Utilization of National Key Laboratory Cultivation Program (20194AFD44003) and Jiangxi Province Key Innovation Research and Development Platform Plan of China (20181BCD40009).

Data Availability All data, models, and code generated or used during the study appear in the submitted article.

Declarations

Conflict of interest On behalf of all authors, the corresponding author states that there is no conflict of interest.

References

[1] Y.B. Yu and W.K. Chow, Review on an advanced high-temperature measurement technology: the optical fiber thermometry. J. Thermodyn., **2009** (2014) 11.
[2] D. Biermann and F. Hollmann, Thermal effects in complex machining processes: final report of the DFG priority program 1480. Springer, Cham (2018).
[3] P. Coates and D. Lowe, The fundamentals of radiation thermometers. CRC Press, Boca Raton (2016).
[4] J.V. Nicholas and D.R. White, Traceable temperatures: an introduction to temperature measurement and calibration, second edition. Meas. Sci. Technol., **13** (2002) 1651.
[5] Z.M. Zhang, B.K. Tsai and G. Machin, Radiometric temperature measurements. Experimental methods in the physical sciences, vol 42. Academic Press, Cambridge (2009).
[6] D.P. Dewitt, Theory and practice of radiation thermometry/ edited by D. P. DeWitt and Gene D. Nutter, (1988).
[7] Schlessinger. Infrared technology fundamentals, second edition. Wine Science (1994) 609–619.
[8] P.R.N. Childs, J.R. Greenwood and C.A. Long, Review of temperature measurement. Rev. Sci. Instrum., **71** (2000) 2959–2978.
[9] L. Bünger, K. Anhalt, R.D. Taubert, U. Krüger and F. Schmidt, Traceability of a CCD-camera system for high-temperature measurements. Int. J. Thermophys., **36** (2015) 1784–1802.
[10] Y.X. Wu, S.H. Shi, J.L. Yu, L.L. Yu and J.J. Wu, The development of temperature measurement system in laser molten pool based on monochrome CCD with high speed. Adv. Mater. Res., **566** (2012) 431–434.
[11] D. Pan, Z. Jiang, Z. Chen, W. Gui, Y. Xie and C. Yang, Temperature measurement and compensation method of blast furnace molten iron based on infrared computer vision. IEEE Trans. Instrum. Meas., **68** (2019) 3576–3588.
[12] Z. Zeng, J.Q. Zhang and Y. Liu, Surface temperature monitoring of casting strand based on CCD image. Adv. Mater. Res., **154–155** (2010) 235–238.
[13] J. Lei, X. Yang, Y. Wang and H. Li, Study on CCD measurement of temperature field in laser molten pool. Lasers Mater. Process. Manuf. II. SPIE, **5629** (2005) 546–556.
[14] D. Ross-Pinnock and P.G. Maropoulos, Review of industrial temperature measurement technologies and research priorities for the thermal characterization of the factories of the future. Proc. Inst. Mech. Eng. Part B: J. Eng. Manuf., **230** (2015) 793–806.
[15] Y. Yu and S.X. Xu, Research on the application technology of linear CCD in dynamic measuring molten tin glass surface. Key Eng. Mater., **381–382** (2008) 169–172.
[16] Z. Cao and X.C. Yang, Measurement of temperature field in laser molten pool by CCD based on DSP. Key Eng. Mater., **392–394** (2008) 693–696.
[17] Z. Xie and H. Bai, Development of three-wavelength CCD image pyrometer used for the temperature field measurements of continuous casting billets. Rev. Sci. Instrum., **85** (2014) 024903.
[18] Y. Zhang, X. Lang, Z. Hu and S. Shu, Development of a CCD-based pyrometer for surface temperature measurement of casting billets. Meas. Sci. Technol., **28** (2017) 065903.
[19] B. Haicheng, Development and application of image pyrometer used for the surface temperature measurements of continuous casting billets. Doctor, University of East North (2013).
[20] S. Liu, S. Liu and G. Tong, Reconstruction method for inversion problems in an acoustic tomography based temperature distribution measurement. Meas. Sci. Technol., **28** (2017) 115005.
[21] Y. Greenberg, E. Yahel, M. Ganor, R. Hevroni, I. Korover, M. Dariel and G. Makov, High precision measurements of the temperature dependence of the sound velocity in selected liquid metals. Non-Cryst. Solids, **354** (2008) 4094–4100.
[22] L. Reindl, I. Shrena, S. Kenshil and R. Peter, Wireless measurement of temperature using surface acoustic waves sensors, in IEEE International Frequency Control Symposium and PDA Exhibition Jointly with the 17th European Frequency and Time Forum, 2003. Proceedings of 2003. IEEE, pp. 935–941 (2003).
[23] B. Scott, C. Willman, B. Williams, P. Ewart, R. Stone and D. Richardson, In-cylinder temperature measurements using laser induced grating spectroscopy and two-colour PLIF. SAE Int. J. Engines, **10** (2017) 2191–2201.
[24] C. Henning, N. Emil, B. Alexis, P. Per, W. Yajing, C. Robert, A. Marcus, B. Per-Erik and B. Xue-Song, Large eddy simulations and rotational CARS/PIV/PLIF measurements of a lean premixed low swirl stabilized flame. Combust and Flame, **161** (2014) 2539–2551.
[25] J. Hwang, Y. Gil, J. Kim, M. Choi and S. Chung, Measurements of temperature and OH radical distributions in a silica generating flame using CARS and PLIF. J. Aerosol Sci., **32** (2001) 601–613.
[26] R. Adityo, R. Agung, P. Satrio and Y.S. Nugroho, Measurement of thermal radiative heat transfer using a multi-axis heat flux sensor, IOP Conference Series: Earth and Environmental Science, 105 (2018).
[27] S. Yatsyshyn, Handbook of Thermometry and Nanothermometry. Lulu.com (2015).
[28] J. Hollandt, J. Hartmann, O. Struß, R. Gärtner, Chapter 1 industrial applications of radiation thermometry, Radiometric temperature measurements: II. Appl. Ser. Exp. Methods Phys. Sci. **43** (2010) 1–56.
[29] D. Crecraft and S. Gergely, Analog electronics: circuits, systems and signal processing. Elsevier Science, Amsterdam (2002).
[30] R. Deeb, D. Muselet, M. Hebert and A. Trémeau, Spectral reflectance estimation from one RGB image using self-interreflections in a concave object. Appl. Opt., **57** (2018) 4918–4929.
[31] H. Lu, L. Ip, A. Mackrory, L. Werrett, J. Scott, D. Tree and L. Baxter, Particle surface temperature measurements with multicolor band pyrometry. AIChE J., **55** (2009) 243–255.

[32] P. Saunders, Radiation thermometry: fundamentals and applications in the petrochemical industry. Society of Photo Optical (2007).
[33] Z.M. Zhang, B.K. Tsai and G. Machin, Radiometric temperature measurements: I. Fundamentals. Elsevier Science, Amsterdam (2009).
[34] T. Larrick, Understanding modern infrared pyrometers for demanding steel mill applications. https://www.deltat.com/pdf/Single-%20Dual-%20and%20Multi-Wavelength%20Infrared%20Thermometer.pdf.
[35] V.C. Raj and S. Prabhu, Measurement of surface temperature and emissivity of different materials by two-colour pyrometry. Rev. Sci. Instrum., **84** (2013) 124903.
[36] C. Purpura, E. Trifoni, M. Musto, G. Rotondo and R. della Ragione, Methodology for spectral emissivity measurement by means of single color pyrometer. Measurement, **82** (2016) 403–409.
[37] Y. Huang, D. Chen, L. Bai, M. Long, K. Lv and P. Xu, Study on the infrared spectral range for radiation temperature measurement of continuous casting slab. EPD Congr., **2016** (2016) 143–151.
[38] L. Cassady and E. Choueiri, High accuracy multi-color pyrometry for high temperature surfaces, in 28th International Electric Propulsion Conference, Toulouse, France, March 2003, pp. 17–21.
[39] S. He, Y. Wang, C. Dai, J. Liu and G. Feng, Analysis and suppression of stray radiation in infrared spectral radiation measurement (Applied Optics and Photonics China (AOPC2019)). SPIE (2019).
[40] Y. Ozaki and R.H. Zee, Investigation of thermal and hydrogen effects on emissivity of refractory metals and carbides. Mater. Sci. Eng.: A, **202** (1995) 134–141.
[41] J. Pujana, L. del Campo, R.B. Pérez-Sáez, M.J. Tello, I. Gallego and P.J. Arrazola, Radiation thermometry applied to temperature measurement in the cutting process. Meas. Sci. Technol., **18** (2007) 3409–3416.
[42] Wikipedia. https://en.wikipedia.org/wiki/Thermography.
[43] J. Shen, Y. Zhang and T. Xing, The study on the measurement accuracy of non-steady state temperature field under different emissivity using infrared thermal image. Infrared Phys. Technol., **94** (2018) 207–213.
[44] Y. Zhang, Z. Wang, X. Fu, F. Yan and T. Kong, An experimental method for improving temperature measurement accuracy of infrared thermal imager. Infrared Phys. Technol., **102** (2019) Art no. Unsp 103020.
[45] Y.-C. Zhang, Y.-M. Chen and C. Luo, A method for improving temperature measurement precision on the uncooled infrared thermal imager. Measurement, **74** (2015) 64–69.
[46] B. Zhao and J.-H. Wang, Ambient temperature compensation of infrared temperature sensor based on PSO-BP. Transducer Microsyst. Technol., **34** (2015) 47–49.
[47] P.R. Muniz, S.P.N. Cani and R.D.S. Magalhaes, Influence of field of view of thermal imagers and angle of view on temperature measurements by infrared thermovision. IEEE Sens. J., **14** (2014) 729–733.
[48] H. Zhang, Z. Jiang, Z. Cheng, W. Gui, Y. Xie and C. Yang, Two-stage control of endpoint temperature for pebble stove combustion. IEEE Access, **7** (2019) 625–640.
[49] D. Pan, Z. Jiang, Z. Chen, W. Gui, Y. Xie and C. Yang, A novel method for compensating temperature measurement error caused by dust using infrared thermal imager. IEEE Sens. J., **19** (2019) 1730–1739.
[50] J. Yang, Z. Xie, Z. Ji and H. Meng, Real-time heat transfer model based on variable non-uniform grid for dynamic control of continuous casting billets. ISIJ Int., **54** (2014) 328–335.
[51] S. Bagavathiappan, B.B. Lahiri, S. Suresh, J. Philip and T. Jayakumar, Online monitoring of cutting tool temperature during micro-end milling using infrared thermography. Insight - Non-Destr. Test. Cond. Monit., **57** (2015) 9–17.
[52] D. Biermann and F. Hollmann, Thermal effects in complex machining processes: final report of the DFG priority programme 1480. Springer, Cham (2017).
[53] N.S. Chernysheva, A.B. Ionov and B.P. Ionov, Usage of dual-channel radiation thermometers in dusty environment, Journal of Physics: Conference Series, vol. 1327 (2019).
[54] D. Hernandez, A. Netchaieff and A. Stein, True temperature measurement on metallic surfaces using a two-color pyroreflectometer method. Rev. Sci. Instrum., **80** (2009) 094903.
[55] J.E. Martin, T.J. Quinn and B. Chu, Further measurements of thermodynamic temperature using a total radiation thermometer: the range – 130 °C to + 60 °C. Metrologia, **25** (1988) 107–112.
[56] T. Quinn and J. Martin, Total radiation measurements of thermodynamic temperature. Metrologia, **33** (1996) 375.
[57] P. Saunders, Radiation thermometry: fundamentals and applications in the petrochemical industry. SPIE Press, Bellingham (2007).
[58] V. Tychowsky and J. Ridge, Development and application of a gold cup sensor for measurement of strip temperatures on a continuous galvanizing line. Iron Steel Eng. (USA), **75** (1998) 37–42.
[59] L. Robins, On-line diagnostics techniques in the oil, gas, and chemical industry, in Proceedings Third Middle East Non-destructive Testing Conference, pp. 27–30 (2005).
[60] N. Depree, J. Sneyd, S. Taylor, M. Taylor, J. Chen, S. Wang and M. O'Connor, Development and validation of models for annealing furnace control from heat transfer fundamentals. Comput. Chem. Eng. **34** (2010) 1849–1853.
[61] G. Machin, K. Anhalt, M. Battuello, F. Bourson, P. Dekkere, A. Diril, F. Edler, C. Elliott, F. Girard, A. Greenen, L. Kňazovickág, D. Lowe, P. Pavlásek, J. Pearce, M. Sadli, R. Strnad, M. Seifert and E. Vuelbane, The European project on high temperature measurement solutions in industry (HiTeMS)—a summary of achievements. Measurement, **78** (2016) 168–179.
[62] N. Depree, J. Sneyd, S. Taylor, M. Taylor, M. OConnor and J. Chen, Mathematical modelling of an annealing furnace for process control applications, ed: Minerals, Metals and Materials Society/AIME, 420 Commonwealth Dr., P. O. Box… (2010).
[63] D.G. Barker and M.R. Jones, Inversion of spectral emission measurements to reconstruct the temperature profile along a blackbody optical fiber thermometer. Inverse Probl. Eng., **11** (2003) 495–513.
[64] Y. Chun-Ling, D. Jing-Min and H. Yan, Optimum identifications of spectral emissivity and temperature for multi-wavelength pyrometry. Chin. Phys. Lett., **20** (2003) 1685.
[65] X. Shenghu, Z. Yongjun, X. Lingyan and X. Dailiang, Uncertainty model and estimation for emissivity of a steel plate with a multi-wavelength pyrometer, in 2009 IEEE Instrumentation and Measurement Technology Conference, pp. 1102–1104 (2009).
[66] P. Wang, Z. Hu, Z. Xie and M. Yan, A new experimental apparatus for emissivity measurements of steel and the application of multi-wavelength thermometry to continuous casting billets. Rev. Sci. Instrum. **89** (2018) 054903.
[67] R. Román, M. Antón, A. Cazorla, A. Miguel, F. Olmo, J. Bilbao and L. Alados-Arboledas, Calibration of an all-sky camera for obtaining sky radiance at three wavelengths. Atmos. Meas. Tech. **5** (2012) 2013–2024.
[68] R.G. Keanini and C. Allgood, Measurement of time varying temperature fields using visible imaging CCD cameras. Int. Commun. Heat Mass Transf., **23** (1996) 305–314.

[69] G. Sutter, L. Faure, A. Molinari, N. Ranc and V. Pina, An experimental technique for the measurement of temperature fields for the orthogonal cutting in high speed machining. Int. J. Mach. Tools Manuf., **43** (2003) 671–678.
[70] E. Renier, F. Meriaudeau, P. Suzeau and F. Truchetet, CCD temperature imaging: applications in steel industry, in Proceedings of the 1996 IEEE IECON. 22nd International Conference on Industrial Electronics, Control, and Instrumentation, vol. 2: IEEE, pp. 1295–1300 (1996).
[71] P.M. Brisley, G. Lu, Y. Yan and S. Cornwell, Three-dimensional temperature measurement of combustion flames using a single monochromatic CCD camera. IEEE Trans. Instrum. Meas., **54** (2005) 1417–1421.
[72] H.-C. Zhou, S.-D. Han, F. Sheng and C.-G. Zheng, Visualization of three-dimensional temperature distributions in a large-scale furnace via regularized reconstruction from radiative energy images: numerical studies. J. Quant. Spectrosc. Radiat. Transf., **72** (2002) 361–383.
[73] M. Shimoda, A. Sugano, T. Kimura, Y. Watanabe and K. Ishiyama, Prediction method of unburnt carbon for coal fired utility boiler using image processing technique of combustion flame. IEEE Trans. Energy Convers., **5** (1990) 640–645.
[74] P.M. Danehy, W.D. Hutchins, T.W. Fahringer and B.S. Thurow, A plenoptic multi-color imaging pyrometer. Presented at the 55th AIAA Aerospace Sciences Meeting (2017).
[75] G. Lu, Y. Yan, G. Riley and H.C. Bheemul, Concurrent measurement of temperature and soot concentration of pulverized coal flames. IEEE Trans. Instrum. Meas., **51** (2002) 990–995.
[76] G. Lu and Y. Yan, Temperature profiling of pulverized coal flames using multicolor pyrometric and digital imaging techniques. IEEE Trans. Instrum. Meas., **55** (2006) 1303–1308.
[77] H. Bai, Z. Xie, Y. Zhang and Z. Hu, Evaluation and improvement in the accuracy of a charge-coupled-device-based pyrometer for temperature field measurements of continuous casting billets. Rev. Sci. Instrum., **84** (2013) 064904.
[78] G. Sparacia and K. Sakai, Temperature measurement by diffusion-weighted imaging. Magn. Resonance Imaging Clin. N. Am., **29** (2021) 253–261.
[79] I. Muttakin and M. Soleimani, Optical conductivity and temperature sensing using magnetic induction spectroscopy imaging. IEEE Trans. Instrum. Meas., **70** (2020) 1–11.
[80] B. Wang, Y. Sun, C. Li, Z. Wang, L. Zhang and X. Wang, 2-D optical temperature measurement of biological samples based on compressive thermoacoustic tomography. IEEE J. Electromagnet. RF Microwaves Med. Biol **5-4** (2021) 371–378.
[81] S. Moller, C. Resagk and C. Cierpka, Long-time experimental investigation of turbulent superstructures in Rayleigh–Bénard convection by optical simultaneous measurements of temperature and velocity fields. Exp. Fluids, **62** (2021) 1–18.
[82] M. Jukiewicz, P. Łupkowski, R. Majchrowski, J. Marcinkowska and D. Ratajczyk, Electrodermal and thermal measurement of users' emotional reaction for a visual stimuli. Case Stud. Thermal Eng., **27** (2021) 101303.
[83] S. Neema, D. Tripathy, S. Mukherjee, A. Sinha, S. Vendhan and B. Vasudevan, Infrared thermography in the diagnosis of palmar hyperhidrosis: a diagnostic study. Med. J. Armed Forces India (2021).
[84] S. Neema, D. Tripathy, S. Mukherjee, A. Sinha, S. Vendhan and B. Vasudevan, The applications of infrared thermography in surgical removal of retained teeth effects assessment. J. Thermal Anal. Calorim., **144** (2021) 139–144.
[85] M.M. Al Qudah, A.S. Mohamed and S.L. Lutfi, Affective state recognition using thermal-based imaging: a survey. Comput. Syst. Sci. Eng., **37** (2021) 47–62.
[86] Z. Sun, B. Parkinson, O. Agbede and K. Hellgardt, Optical differential pressure technique for bubble characterization in high-temperature opaque systems. Ind. Eng. Chem. Res., **59** (2020) 6236–6246.
[87] X. Wang, X. Wang, X. Cheng and H. Yang, A novel ratiometric fluorescent thermometer based on ZIF-8 thin films. Mater. Lett., **306** (2021) 131051.
[88] S. Yuan, S. Zhao, L. Lou, D. Zhu, Z. Mu and F. Wu, Fluorescence intensity ratio optical thermometer $YNbO_4$:Pr^{3+}, Tb^{3+} based on intervalence charge transfer. Powder Technol., **395** (2022) 83–92.
[89] D.S. Lee and J.H. Jo, Application of IR camera and pyranometer for estimation of longwave and shortwave mean radiant temperatures at multiple locations. Build. Environ., **207** (2021) 108423.
[90] L. Marciniak, W. Piotrowski, M. Szalkowski, V. Kinzhybalo, M. Drozd, M. Dramicanin and A. Bednarkiewicz, Highly sensitive luminescence nanothermometry and thermal imaging facilitated by phase transition. Chem. Eng. J., **427** (2022) 131941.
[91] C. Urano, K. Yamazawa and N.-H. Kaneko, Measurement of the melting point of gallium using a Johnson noise thermometer. IEEE Trans. Instrum. Meas., **69** (2019) 3698–3703.
[92] C. Kirmse and H. Chaves, Measurement of the average two-dimensional surface temperature distribution of drops in a melt atomization process. J. Thermal Spray Technol., **24** (2015) 690–695.
[93] M. Han, J. Nie, K. Sun, X. Wang and X. Dou, Experiment on the temporal evolution characteristics of a CCD multilayer structure irradiated by a 1.06 μm continuous laser. Appl. Opt., **57** (2018) 4415–4420.
[94] Li. Hui and Wang Chuan-Bing, Measurement of cathode surface temperature using the method of CCD imaging in arc discharge. Nuclear Sci. Tech., **17** (2006) 237–240.
[95] A. Huber, D. Kinna, V. Huber, G. Arnoux, G. Sergienko, I. Balboa and K. Zastrow, Real-time protection of the JET ITER-like wall based on near infrared imaging diagnostic systems. Nuclear Fusion, **58** (2018) 106021.
[96] J. Fang, H. Zhang, G. Wu, Y. Chen and P. Xue, Temperature field measurement of plasma stream during rapid sprayed tooling. Optical measurement and nondestructive testing: techniques and applications. Int. Soc. Opt. Photon. **4221** (2000) 310–314.
[97] Z. Zeng, J.Q. Zhang and Y. Liu, Surface temperature monitoring of casting strand based on CCD image. Advanced Materials Research, vol. 154. Trans Tech Publications Ltd (2011).
[98] J. Yan and W. Li, Research on colorimetric temperature-measurement method improved based on CCD imaging, 2010 3rd international congress on image and signal processing, vol. 1. IEEE (2010).
[99] Y. Li, S. Li and K. Ye, Design and implementation of a soft-measuring system for high-temperature field based on color CCD image sensor. ECS Trans., **45** (2013) 27.
[100] L. Wu and G. Cai, Soft sensor method of temperature measurement using CCD image color based on LS-SVM. Energy Procedia, **13** (2011) 2229–2235.
[101] Y. Wu, Y. Hu, F. Jiang and L. Zhang, Design of temperature measurement system based on two-color imaging in adaptive optics of CCD, 5th International Symposium on Advanced Optical Manufacturing and Testing Technologies: Optical Test and Measurement Technology and Equipment, **7656** (2010) 1062–1067.